American Mineralogist, Volume 94, pages 785–792, 2009

The occurrence of tetrahedrally coordinated Al and B in tourmaline: An ^{11}B and ^{27}Al MAS NMR study

Aaron J. Lussier,[1] Pedro M. Aguiar,[2] Vladimir K. Michaelis,[2] Scott Kroeker,[2] and Frank C. Hawthorne[1,*]

[1]Department of Geological Sciences, University of Manitoba, Winnipeg, Manitoba R3T 2N2, Canada
[2]Department of Chemistry, University of Manitoba, Winnipeg, Manitoba R3T 2N2, Canada

Abstract

Considerable uncertainty has surrounded the occurrence of tetrahedrally coordinated Al and B at the *T* site in tourmaline. Although previously detected in several tourmaline specimens, the frequency of these substitutions in nature, as well as the extent to which they occur in the tourmaline structure, is not known. Using ^{11}B and ^{27}Al MAS NMR spectroscopy, we have investigated the presence of B and Al at the *T* site in 50 inclusion-free tourmaline specimens of low transition-metal content and different species (elbaite, "fluor-elbaite," liddicoatite, dravite, uvite, olenite, and magnesiofoitite) from different localities worldwide. Chemical shifts of $^{[4]}B$ and $^{[3]}B$ in ^{11}B spectra, and $^{[4]}Al$ and $^{[6]}Al$ in ^{27}Al spectra, are well resolved, allowing detection of even small amounts of *T*-site constituents. In the observed spectra, $^{[4]}B$ and $^{[3]}B$ peaks are located at 0 and 18–20 ppm, respectively, with the greatest intensity corresponding to $^{[3]}B$ (=3 apfu). In ^{27}Al spectra, $^{[4]}Al$ and $^{[6]}Al$ bands are located at 68–72 and 0 ppm, respectively, with the greater intensity corresponding to $^{[6]}Al$. However, inadequate separation of ^{Y}Al and ^{Z}Al precludes resolution of these two bands. Simulation of ^{11}B MAS NMR spectra shows that tetrahedrally and trigonally coordinated B can be readily distinguished at 14.1 T and that a $^{[4]}B$ content of 0.0–0.5 apfu is common in tourmaline containing low amounts of paramagnetic species. ^{27}Al MAS NMR spectra show that Al is also a common constituent of the *T* site in tourmaline. Determination of $^{[4]}Al$ content by peak-area integration commonly shows values of 0.0–0.5 apfu. Furthermore, the chemical shift of the ^{27}Al tetrahedral peak is sensitive to local order at the adjacent *Y* and *Z* octahedra, where $^{[4]}Al$-$^{Y}Mg_3$ and $^{[4]}Al$-$^{Y}(Al,Li)_3$ arrangements result in peaks located at ~65 and ~75 ppm, respectively. Both ^{11}B MAS NMR and ^{27}Al MAS NMR spectra show peak broadening as a function of transition-metal content (i.e., $Mn^{2+} + Fe^{2+}$ = 0.01–0.30 apfu) in the host tourmaline. In ^{11}B spectra, broadening and loss of intensity of the $^{[3]}B$ signal ultimately obscures the signal corresponding to $^{[4]}B$, increasing the limit of detection of $^{[4]}B$ in tourmaline. Our results clearly show that all combinations of Si, Al, and B: $T = (Al, Si)_6$, $T = (B, Si)_6$, $T = (Al, B, Si)_6$, and $T = Si_6$ apfu, are common in natural tourmalines.

Keywords: Tourmaline, ^{11}B and ^{27}Al MAS NMR, tetrahedrally coordinated B and Al

Introduction

The general formula of the tourmaline-group minerals may be written as

$$X\,Y_3\,Z_6\,T_6\,O_{18}\,(BO_3)_3\,V_3\,W$$

where X = Na, Ca, K, and □ (vacancy); Y = Mg, Fe^{2+}, Mn^{2+}, Al, Fe^{3+}, Cr^{3+}, V^{3+}, Ti^{4+}, and Li; Z = Al, Fe^{3+}, Cr^{3+}, V^{3+}, and Mg; T = Si, Al, and B; V = O^{2-} and OH; W = OH, F, and O^{2-} (Hawthorne and Henry 1999). Tourmaline can provide a record of progressive metamorphism (Henry and Dutrow 1992, 1996; Henry and Guidotti 1985; Povondra and Novàk 1986) and sequential crystallization in granites and granitic pegmatites (Aurisicchio et al. 1999; Dyar et al. 1998; Novàk et al. 1999; Selway et al. 1998, 1999, 2000a, 2000b, 2002; Neiva et al. 2007). However, there are still uncertainties in our knowledge of the crystal chemistry of tourmaline. Until relatively recently, it was thought that only Al (Povondra 1981; Grice and Ercit 1993) could substitute for Si in the tourmaline structure. However, it has since been shown directly that B may occur in tetrahedral coordination in tourmaline (Tagg et al. 1999; Schreyer et al. 2000; Marler and Ertl 2002). However, it is still unknown whether $^{[4]}B$ (tetrahedrally coordinated B) is a common constituent in tourmaline, and whether it is restricted to certain species of tourmaline, or to specific geologic environments. Moreover, it is still commonplace to calculate tourmaline formulae by setting B = 3 apfu (i.e., only $^{[3]}B$ is assumed to be present) and $^{[4]}Al = 6 - Si$ apfu. Any error introduced into the unit formula by this approach is typically obscured by the fact that the light elements (i.e., Li_2O, B_2O_3, and H_2O) are usually calculated using stoichiometric constraints, and Fe^{3+} contents are estimated by electroneutrality and stoichiometry assumptions, or assumed to be zero. Can we ignore $^{[4]}B$, unless it

* E-mail: frank_hawthorne@umanitoba.ca

0003-004X/09/0506–785$05.00/DOI: 10.2138/am.2009.3000

has been shown to be present, or must we come to grips with the fact that it is a common constituent of tourmaline? This question impacts the systematic chemical-analytical work on tourmaline in the wide variety of rocks in which it occurs, and the work reported here addresses this question.

Here, we use ^{11}B and ^{27}Al magic-angle-spinning nuclear magnetic resonance (MAS NMR) spectroscopy to investigate the occurrence of tetrahedrally coordinated constituents in a large suite of low-(Fe,Mn) tourmalines of various compositions. Previous ^{11}B MAS NMR work has examined elbaite or olenite, and many of the specimens examined in the present study are the same species because elbaite or olenite can be sufficiently low in paramagnetic constituents to obtain good-quality MAS NMR spectra. Some samples from the present work correspond to other compositions (magnesiofoitite, schorl, "fluor-elbaite," liddicoatite, uvite), but it is difficult to find samples sufficiently low in paramagnetic species for MAS NMR spectroscopy.

Previous work

MAS NMR spectroscopy is a powerful method for determining coordination numbers of elements in solids. Boron (^{11}B) and Al (^{27}Al) are of particular interest with regard to tourmaline. $^{[3]}$B and $^{[4]}$B have chemical shifts of 12 to 19 ppm and –4 to 2 ppm, respectively (Bray et al. 1961; Turner et al. 1986), and $^{[4]}$Al and $^{[6]}$Al have chemical shifts of 50 to 80 ppm and –10 to 15 ppm, respectively (Kirkpatrick 1988; Kirkpatrick et al. 1985, 1986). Thus coordination numbers, and hence site assignments, can be determined, provided the structure does not contain sufficient paramagnetic species (particularly transition metals) to attenuate the signal. ^{11}B MAS NMR has been used for the detection of $^{[4]}$B in tourmaline. Tagg et al. (1999) reported small amounts (0.1–0.2 apfu) of $^{[4]}$B in elbaite, showing that at low field (7.05 T), there is overlap between the peaks for $^{[3]}$B and $^{[4]}$B, whereas at higher field (11.74 T), the peaks are well resolved. Schreyer et al. (2000) and Marler and Ertl (2002) reported low-field ^{11}B MAS NMR spectra of a synthetic olenite with a nominal *T*-site content of Si_3B_3, and a $^{[4]}$B-bearing olenite from a granitic pegmatite. Ertl et al. (1997) and Hughes et al. (2000, 2001) have shown that <*T*-O> distances in the tourmaline examined by Marler and Ertl (2002) are in accord with the presence of $^{[4]}$B, and similar stereochemical results have been reported (Hughes et al. 2004; Kalt et al. 2001; Marler et al. 2002; Ertl et al. 2005, 2006, 2007) indicating the presence of $^{[4]}$B in Li-bearing tourmaline.

To date, MAS NMR has not been applied to the investigation of $^{[4]}$Al (tetrahedrally coordinated Al) in tourmaline, despite the fact that it is amenable to the task, as both [4]- and [6]-coordinated Al differ sufficiently in resonance frequency (50 to 80 and –10 to 15 ppm, respectively) to provide good resolution at the moderately high field used here, even at small $^{[4]}$Al/$^{[4+6]}$Al ratios. MacDonald and Hawthorne (1995) have shown that <*T*-O> distances in uvite, ideally $Ca(Mg,Fe^{2+})_3(MgAl_5)Si_6O_{18}(BO_3)_3(F,OH)_4$, are in accord with the occurrence of Al at the *T* site, and structural work on other compositions (Bloodaxe et al. 1999; Schreyer et al. 2002; Cempírek et al. 2006; Prowatke et al. 2003; Ertl and Hughes 2002; Ertl et al. 2003) also show small amounts of Al at the *T* site.

Single-crystal structure refinements suggest that the <*T*-O> distance in tourmaline is sensitive to the presence of $^{[4]}$B (Hughes et al. 2000, 2004; Ertl et al. 1997, 2005, 2006, 2007). However, this type of relation is not yet at the stage of being a predictive compositional tool, partly because of the possibility that Al may also occur at the *T* site and perturb any possible relation between <*T*-O> and $^{[4]}$B content. Kalt et al. (2001) and Ertl et al. (2005) report the occurrence of Al and B (as well as Si) at the *T* site in Li-rich tourmalines based on direct analysis of B, but this type of site assignment is imprecise as it relies on the accurate analysis of B, and uncertainties in the determination of B are ~10% relative.

Experimental methods

Samples

A total of 50 tourmaline crystals were assembled for MAS NMR spectroscopy from various localities (Table 1). Investigation by MAS NMR requires that the samples be as free of transition metals as possible, due to the fact that paramagnetic species can induce very fast relaxation of the nuclear spins, broadening the resonance signal. This limitation restricts this investigation to Li-Al tourmalines: liddicoatite, elbaite ("fluor-elbaite"), rossmanite, and olenite, and low-Fe dravite, uvite, and magnesiofoitite. The *X*-site concentrations of samples examined here are summarized in Figure 1. We examined each sample very carefully for inclusions and discarded any grains that had optically visible solid inclusions or extraneous material adhering to grain boundaries. Lussier et al. (2008a, 2008b) show that variation in $^{[4]}$B correlates with other chemical variations in tourmaline that maintain electroneutrality; such correlations would not be expected if the presence of $^{[4]}$B were due to the presence of an extraneous phase.

Chemical analysis

Sample compositions were analyzed with a Cameca SX-100 electron microprobe operating in wavelength-dispersion mode with an accelerating voltage of 15 kV, a specimen current of 15 nA, and a beam diameter of 10 μm. Analyses were done on single grains (5–10 EMPA analysis points per grain) extracted from the larger samples. For samples where further compositional constraint was needed due to zoning, the powdered crystallites used in the MAS NMR experiments were set in epoxy, polished and analyzed (10–15 points). In most cases, the following elements were analyzed: Si, Al, Na, Ca, Fe, Mn, Mg, Ti, Pb, V, Cr, Zn, and F. The following standards and spectrometer crystals were used for $K\alpha$ spectral lines.

TAP: Na, albite; Al, kyanite; Si, diopside;
LTAP: F, F-riebeckite; Mg, forsterite;
LPET: K, orthoclase; Ca, diopside; Ti, titanite; Pb, PbTe;
LLiF: Fe, fayalite; Mn, spessartine.

Accurate and precise analysis of H, Li, and B in tourmaline is difficult to impossible with current instrumentation. In particular, the identification of B in excess of 3 apfu is difficult because there is a relatively large amount of $^{[3]}$B present in the structure, and small amounts of of $^{[4]}$B can be obscured by (statistical) analytical uncertainty in the total B content. The Li content is often calculated by the following relation: ^{Y}Li = 3 – Σ*Y* apfu, and X-ray scattering (Burns et al. 1994, this work) is generally compatible with this calculation for Li-rich tourmalines. The H content is usually calculated as OH + F = 4 apfu. This assumes that there are only monovalent anions at the O1 or O3 sites. This is not necessarily true. Taylor et al. (1995) have shown that the presence of O^{2-} at O1 correlates with the occurrence of Mg at *Z* and Al at *Y*, and hence the latter are indicative of OH + F ≠ 4 apfu. Here, unit formulae were calculated based on 31 anions per formula unit, with ^{Y}Li = 3 – Σ*Y* apfu, and OH + F = 4 apfu. Chemical compositions are given in Table 2[1].

[1] Deposit item AM-09-024, Table 2 (Chemical compositions). Deposit items are available two ways: For a paper copy contact the Business Office of the Mineralogical Society of America (see inside front cover of recent issue) for price information. For an electronic copy visit the MSA web site at http://www.minsocam.org, go to the American Mineralogist Contents, find the table of contents for the specific volume/issue wanted, and then click on the deposit link there.

Table 1. List of tourmaline samples investigated by ^{11}B and ^{27}Al MAS NMR, colors, localities, and *T*-site occupancies

Sample	Species	Locality	Color	Source*	Sample no.
		$^{[4]}$B, $^{[4]}$Al, and Si present			
AT6	Elbaite	Black Rapids Glacier, Alaska	Light pink	a	BRP
AT7	Liddicoatite	Black Rapids Glacier, Alaska	Light green	a	BRG
AT9	"Fluor-elbaite"	Moravia, Czech Republic	Pale pink	a	LA 7–1 CR
AT10	Elbaite	Pesrig, Saxony, Germany	Pink/purple	b	T48 / M6101
AT14	Olenite	Koralpe, Austria	Colorless/pale green	g	–
AT16	Liddicoatite	Namibia	Dark pink to colorless	a	NT3
AT18	Liddicoatite	Namibia	Light pink	a	NT5
AT19	Liddicoatite	Namibia	Light pink/green/orange	a	NT6
AT20	Liddicoatite	Namibia	Pink	a	NT7
AT21	Liddicoatite	Namibia	Pink	a	NT8
AT28	Elbaite	Pala, California	Light pink	a	–
AT50	Olenite	Belo Horizonte, California	Colorless	a	–
AT51	Olenite	Nina La Verda, Brazil	Colorless	a	–
AT52	Elbaite	Sverdlouskoblast, Ural Mts., USSR	Pink	e	T15
AT54	Elbaite	Tanco Pegmatite, Manitoba	Pink	f	T34
AT73	Elbaite	Mogok, Myanmar	Pink	a	SHM1
AT73	Elbaite	Mogok, Myanmar	Colorless	a	SHM2
AT75	Elbaite	Mogok, Myanmar	Purple/colorless	a	SHW2
		$^{[4]}$Al and Si present			
AT13	Dravite	Brandu Valley, Pakistan	Honey brown	a	–
AT53	Uvite	Laxton Twp, Ontario	Pink	b	T23 / M20414
AT55	Dravite	Karsten, Germany	Golden brown	b	T42 / M19631
AT57	Uvite	Franklin, New Jersey	Green	c	T59 / C80699
AT58	Dravite	Darau Stazh, SW Pamirs	Colorless	h	T69 / DC080813
AT59	Uvite	East Africa	Green	a	T73
AT60	Uvite	East Africa	Green	a	T75
AT61	Uvite	East Africa	Green	a	T79
AT63	Dravite	Tanzania	Green	d	T85 / 143901
AT65	Elbaite	Brazil	Pink	a	T96
AT67	Uvite	Burma	Dark green	a	133839
AT68	Uvite	East Africa	Green	a	T78
AT70	Mg-foitite	Kyonosawa, Japan	Pale gray/colorless	a	–
AT72	Dravite	Morogoro, Tanzania	Pale brown/colorless	a	–
		$^{[4]}$B and Si present			
AT47	Liddicoatite	Namibia	Dark green to colorless	a	NT13
AT56	Elbaite	Elba, Italy	Colorless	b	T47 / E1454
AT75	Elbaite	Mogok, Myanmar	Pinkish purple	a	SHW1
		Si present			
AT11	Elbaite	Minas Gerais, Brazil	Light green	b	T50 / M31184
AT48	Liddicoatite	Namibia	Green	a	NT14
AT49	Elbaite	Namibia	Pale green	a	NT15
AT66	Liddicoatite	Madagascar	Colorless	d	T98 / T98m / 165836
AT71	Liddicoatite	Anjanbonoina Pegmatite- Madagascar	Light green	i	NMR1
AT71	Liddicoatite	Anjanbonoina Pegmatite- Madagascar	Light purple	i	NMR7
AT71	Liddicoatite	Anjanbonoina Pegmatite- Madagascar	Dark purple	i	NMR9
AT71	Elbaite	Anjanbonoina Pegmatite- Madagascar	Dark purple	i	NMR10
		Unresolvable			
AT17	Liddicoatite	Namibia	Dark pink	a	NT4
AT23	Liddicoatite	Namibia	Light pink/colorless	a	NT10
AT25	Elbaite	Namibia	Light pink/colorless	a	NT12
AT62	Elbaite	Brazil	Green	a	T83
AT64	"Fluor-elbaite"	San Diego County, California	Pale yellow/green	j	T94 / T94m
AT73	Elbaite	Mogok, Myanmar	Black	a	SHM3
AT76	Elbaite	Astor, Pakistan	Pale green	a	MT16

*a = Frank C. Hawthorne, University of Manitoba; b = Royal Ontario Museum, Ottawa, Canada; c = American Museum of Natural History; d = Smithsonian Institute, Washington; e = National Museum of Natural Sciences; f = Mark Cooper, University of Manitoba; g = Andreas Ertl; h = Edward S. Grew; i = Carl Francis, Harvard University; j = Dalhousie University.

MAS NMR

A Varian Inova 600 spectrometer (14.1 T) was used to record the MAS NMR spectra of ^{27}Al (ν_L = 156.3 MHz) and ^{11}B (ν_L = 192.4 MHz) in all tourmaline samples. For each sample, weighed amounts (10–35 mg) of powdered sample (~15 μm crystallites) were placed in a 3.2 mm (22 μL capacity) zirconia rotor and spun at speeds of 20–24 kHz in a double-resonance probe. The optimized recycle delay was determined independently for each sample; averages were 5 and 30 s for ^{27}Al and ^{11}B, respectively. The final spectra are composites of 512–3072 averaged scans. Spectra were referenced to 0.1 *M* H_3BO_3 as a secondary reference [= +19.6 ppm with respect to $BF_3(CH_3CH_2)_2O$], and 1.1 *M* $Al(NO_3)_3$. Pulse widths were selected to coincide approximately with a 20° tip angle at an rf nutation frequency of 50 kHz.

Results: ^{11}B MAS NMR

Selected ^{11}B MAS NMR spectra are shown in Figure 2 and clearly illustrate the ability of the MAS NMR to resolve [3]- and [4]-coordinated B at higher field (14.1 T), in accord with Tagg et al. (1999). The peak for B in triangular coordination has a characteristic quadrupolar lineshape with δ_{iso} ~18–20 ppm, whereas the peaks for B in tetrahedral coordination are significantly narrower and occur at δ_{iso} ~0 ppm (Bray 1999; Bray et al. 1961; Turner et al. 1986; Kroeker et al. 2001; Kroeker and Stebbins 2001).

^{11}B MAS NMR spectra were calculated using the time-domain

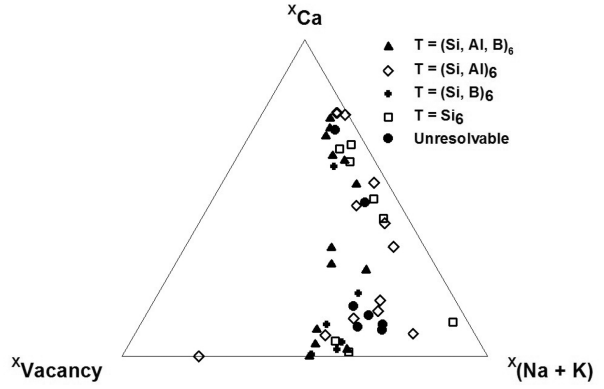

FIGURE 1. Variation in occupancy of the *X* site in the tourmalines of this study; the symbols indicate the type of *T*-site occupancy for each tourmaline.

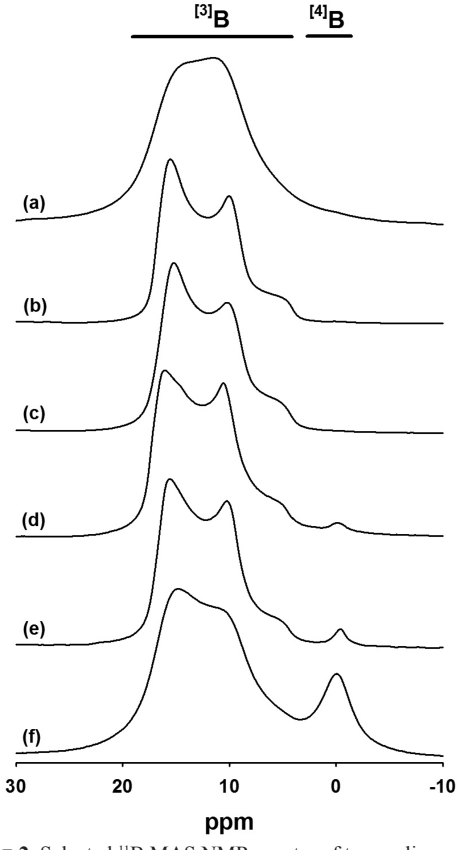

FIGURE 2. Selected ^{11}B MAS NMR spectra of tourmalines ranging from 0.0–0.5 apfu $^{[4]}$B as determined by spectral simulation: (**a**) Mg-foitite (AT70), (**b**) uvite (AT59), (**c**) dravite (AT72), (**d**) liddicoatite (AT20), (**e**) elbaite (AT52), (**f**) olenite (AT14). All spectra are scaled to the same height to facilitate comparison.

density-matrix calculation program, STARS (Skibsted et al. 1991), as implemented in the spectrometer software. Isotropic chemical shifts, quadrupole coupling constants, and quadrupolar asymmetry parameters were obtained, as appropriate, for the different boron sites by manual adjustment of these NMR parameters for all transitions, in addition to the relative amplitude and line-broadening functions. The ^{27}Al MAS NMR spectra lack the well-defined lineshapes required to obtain NMR parameters, but could be faithfully modeled by asymmetric Lorentzian-Gaussian peakshapes, from which the integrated intensities could be reliably determined. In both cases, fits were evaluated by visual comparison between experimental and calculated spectra, and uncertainties assessed by altering given parameters to the threshold of reasonable agreement. Errors are estimated as ±0.05 apfu for B and ±0.08 apfu for Al as site populations. An example of spectral simulation for Koralpe olenite (AT14) is shown in Figure 3. Values for quadrupolar NMR parameters (i.e., Cq and η) and δ_{iso} were determined for each sample by optimization, beginning with the values given for elbaite and dravite by Tagg et al. (1999). Chemical-shift anisotropy (CSA) was ignored, following the findings of Tagg et al. (1999) and Marler and Ertl (2002) that this parameter does not significantly affect the lineshape of the central $^{[3]}$B transition. Lorentzian line-broadening (100–400 Hz) was added to improve agreement between the observed and simulated spectra and obtain reliable integrated intensities representing relative site populations. Intensities are converted into site populations as follows. (1) Boron: $^{[4]}B/(^{[3]}B + ^{[4]}B) = {}^{[4]}I^{B}/({}^{[3]}I^{B} + {}^{[4]}I^{B})$ where $^{[4]}I^{B}$ is the absolute intensity of the MAS NMR peak for $^{[4]}$B; the amount of $^{[3]}$B is fixed stoichiometrically at 3.0 apfu, and hence the above equation may be rearranged to give $^{[4]}B = 3 \times {}^{[4]}I^{B}/{}^{[3]}I^{B}$ apfu. (2) Aluminum: $^{[4]}Al/(^{[4]}Al + {}^{[6]}Al) = {}^{[4]}I^{Al}/({}^{[4]}I^{Al} + {}^{[6]}I^{Al})$ where $^{[4]}I^{Al}$ is the absolute intensity of the MAS NMR peak for $^{[4]}$Al; the total amount of Al, $(^{[4]}Al + {}^{[6]}Al) = Al^{total}$, is determined by normalization of the electron microprobe analysis to give the chemical formula, and hence the above equation may be rearranged to give $^{[4]}Al = Al^{total} \times {}^{[4]}I^{Al}/({}^{[4]}I^{Al} + {}^{[6]}I^{Al})$ apfu. The results are given in Table 3.

RESULTS: ^{27}AL MAS NMR

Typical examples of ^{27}Al MAS NMR spectra of tourmalines with very low paramagnetic constituents are shown in Figure 4. All spectra show a very strong peak close to 0 ppm, characteristic of $^{[6]}$Al, as expected, given that Al completely occupies the [6]-coordinated *Z* site in all specimens examined here. Most spectra show a weak peak at ~65–80 ppm, characteristic of $^{[4]}$Al, whereas

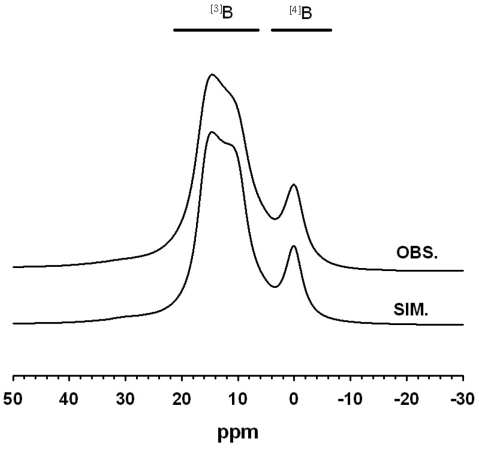

FIGURE 3. Example of an ^{11}B spectral simulation for Koralpe olenite. Final NMR parameters are as follows: BO_3, δ_{iso} = 18.1 ppm, Cq = 2.89 MHz, η = 0.15; BO_4, δ_{iso} = –0.1 ppm, Cq = 0.2 MHz, η = 0.8.

TABLE 3. Calculated percentages of tetrahedral occupants

	Species	$^{[4]}$B (apfu)*	$^{[4]}$Al (apfu)†
AT6	Elbaite	<0.03	<0.08
AT7	Liddicoatite	<0.03	<0.07
AT9	"Fluor-elbaite"	0.06	0.20
AT10	Elbaite	0.03	0.10
AT13	Dravite	–	0.10
AT14	Olenite	0.45	0.26
AT16	Liddicoatite	0.06	<0.07
AT18	Liddicoatite	0.05	<0.07
AT19	Liddicoatite	0.05	<0.07
AT20	Liddicoatite	<0.03	<0.07
AT21	Liddicoatite	<0.03	tr
AT28	Elbaite	0.12	0.08
AT47	Liddicoatite	0.05	–
AT50	Olenite	0.30	0.13
AT51	Olenite	0.39	0.11
AT52	Elbaite	0.06	0.15
AT53	Uvite	–	0.11
AT54	Elbaite	<0.03	0.18
AT55	Dravite	–	0.09
AT56	Elbaite	0.12	–
AT57	Uvite	–	tr
AT58	Dravite	–	<0.06
AT59	Uvite	–	0.28
AT60	Uvite	–	0.45
AT61	Uvite	–	0.18
AT63	Dravite	–	0.19
AT65	Elbaite	–	tr
AT67	Uvite	–	0.11
AT68	Uvite	–	0.25
AT70	Mg-foitite	–	<0.07
AT72	Dravite	–	<0.07
AT73(SHM1)	Elbaite	0.13	<0.08
AT73(SHM2)	Elbaite	0.13	<0.08
AT75(SHW1)	Elbaite	0.19	–
AT75(SHW2)	Elbaite	0.23	0.34

* Simulation using STARS.
† Peak-fitting.

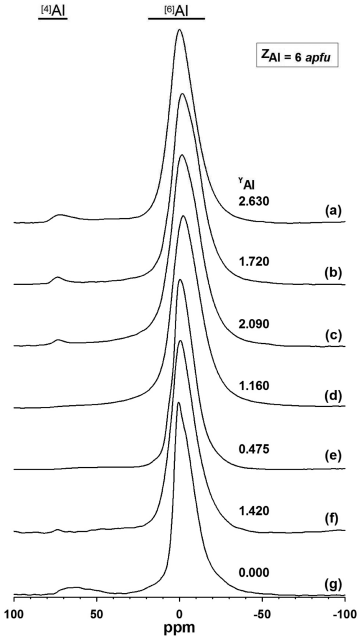

FIGURE 4. Selected ^{27}Al MAS NMR spectra: (**a**) olenite (AT14), (**b**) "fluor-elbaite" (AT9), (**c**) elbaite (AT10), (**d**) liddicoatite (AT20), (**e**) dravite (AT72), (**f**) magnesiofoitite (AT70), (**g**) uvite (AT61); the regions characteristic of $^{[4]}$Al and $^{[6]}$Al are marked. All spectra are scaled to the same height to facilitate comparison.

the spectrum of a liddicoatite (Fig. 4d) shows no such signal, indicating that there is no $^{[4]}$Al present in this specimen.

$^{[4]}$Al in tourmaline

The spectral range of signals from $^{[4]}$Al in several samples is shown enlarged in Figure 5. It is apparent that there is significant variation in peak shape and position. In the tourmaline structure, the *T* tetrahedron shares corners with one *Y* octahedron and two *Z* octahedra, and the two additional anions link to the *X* cation (Fig. 6). As ^{27}Al MAS NMR is sensitive to small differences in local atomic arrangement (Klinowski et al. 1987), it should be possible to detect the difference between $^{[4]}$Al in dravite and uvite,

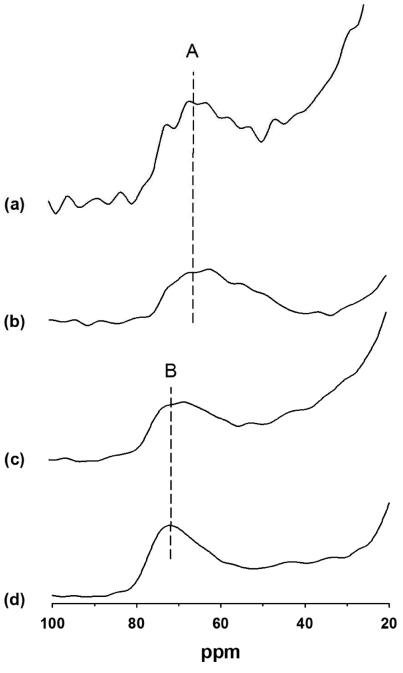

FIGURE 5. ^{27}Al MAS NMR spectra showing the $^{[4]}$Al region in (**a**) uvite (AT57), (**b**) uvite (AT60), (**c**) elbaite (AT54), and (**d**) olenite (AT14). The lines A and B are drawn to emphasize the difference in position of the peaks in the spectra.

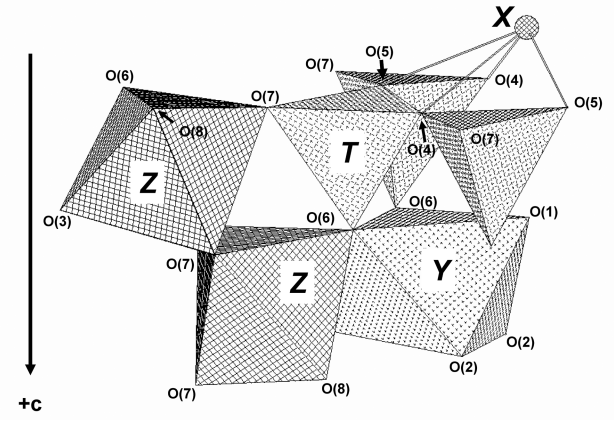

FIGURE 6. Local environment around the *T* site in tourmaline; *Z* octahedron = orthogonal cross-hatched pattern, *Y* octahedron = crosses, and tetrahedra = decorated square net.

in which the *Z* site is occupied by Al and Mg and the *Y* site is occupied by Mg, and elbaite and liddicoatite, in which the *Z* site is occupied only by Al, and the *Y* site is occupied by Al and Li. This is indeed the case. For tourmaline, in which $Y_3 = Mg_3$, the $^{[4]}$Al peak is 68 ppm, whereas for tourmaline in which $Y = (Al, Li)_3$, the $^{[4]}$Al peak occurs at ~72 ppm (Fig. 5).

$^{[6]}$Al in tourmaline

In tourmaline, we expect signals for $^{[6]}$Al from ^{Y}Al and ^{Z}Al. The ^{27}Al MAS NMR spectrum of transition-metal-free uvite (AT61) is shown in Figure 4g. MacDonald and Hawthorne (1995) investigated this sample, as well as several other uvite samples, by crystal-structure refinement and electron-microprobe analysis. Site assignments are in accord with the variation in bond lengths, indicating that $^{[6]}$Al occurs only at the *Z* site, and Mg occupies both the *Y* site and the *Z* site. Given that Al is minimally disordered in this structure, only a single prominent $^{[6]}$Al peak should be observed in the ^{27}Al MAS spectrum, and in accord with this pattern of order, AT61 shows the smallest peakwidth of all the spectra in Figure 4.

The spectra in Figure 4 show a subtle variation in the profile of the envelope centered at 0 ppm. Some peaks (such as g) are narrow and asymmetric, whereas other peaks are broader and symmetric. To the right of each spectrum is shown the amount of ^{Y}Al in that particular tourmaline; values range from 0.0 to 2.63 apfu. As the *Z* site is completely filled with Al in all the specimens included in Figure 4, we must conclude that the width of the peak centered on 0 ppm increases with increasing Al content of the *Y* site. There are two possible causes for this: (1) the envelope centered on 0 ppm contains two discrete peaks with slightly different values of chemical shift; and (2) there is increasing quadrupolar broadening with increasing Al content of the *Y* site. It is not possible to distinguish between these two possibilities here, but it is probable that both contribute to the increasing peak width in Figure 4.

The effect of paramagnetic constituents

Figure 7 compares the ^{27}Al and ^{11}B MAS NMR spectra of elbaite-liddicoatite with different contents of paramagnetic constituents (i.e., $Fe^{2+} + Mn^{2+} = 0.01$–0.30 apfu; Table 2[1]). Cursory inspection of these spectra indicates that increasing amounts of paramagnetic constituents result in dramatic changes to the spectral intensity. The integrated peak intensities of the spectra (which were all collected under identical experimental conditions on weighed amounts of sample) diminish dramatically with the incorporation of paramagnetic components in the tourmaline. Inspection of Figure 7 suggests that the response of the ^{27}Al and ^{11}B spectra to paramagnetic broadening is the same, and this is confirmed by comparison of the relative intensities of the different spectra in each sample (Fig. 8); the data scatter closely about the 1:1 line.

Occurrence of tetrahedrally coordinated constituents in tourmaline

The results of this work are summarized in Table 3. In Table 1, the specimens are separated into four groups on the basis of the *T*-site species present: (1) $T = Si_6$ apfu; (2) $T = (Si + B)_6$ apfu; (3) $T = (Si + Al)_6$ apfu; and (4) $T = (Si + B + Al)_6$ apfu.

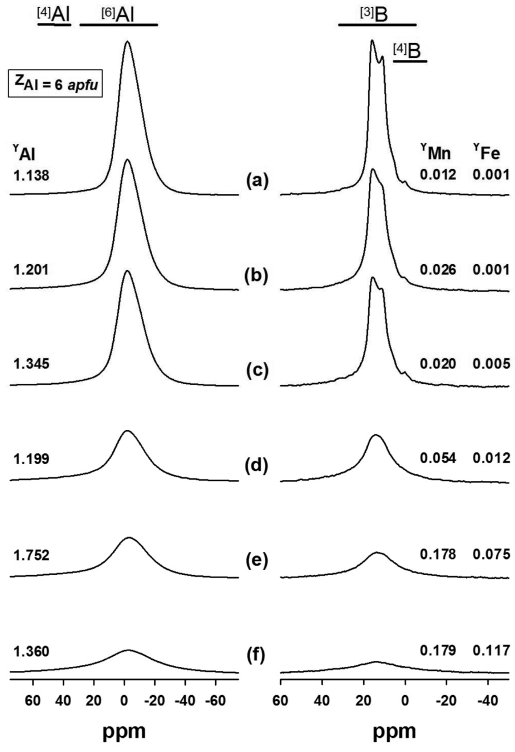

FIGURE 7. ^{27}Al and ^{11}B MAS NMR spectra of elbaite-liddicoatite with differing contents of paramagnetic constituents: (**a**) AT21; (**b**) AT18; (**c**) AT16; (**d**) AT23; (**e**) AT48; (**f**) AT17. All spectra are on the same scale.

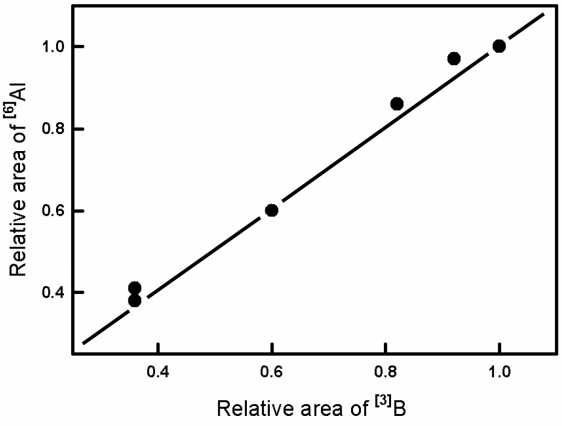

FIGURE 8. Comparison of the relative areas of the ^{27}Al and ^{11}B MAS spectra of elbaite-liddicoatite shown in Figure 7. The data scatter about the 1:1 line, indicating that they are equally affected by paramagnetic quenching.

Upon inspection of Table 1, it is immediately apparent that the tetrahedrally coordinated constituents of tourmaline are more variable than was previously realized. Of the 50 individual samples investigated, eight have $T = 6$ Si apfu, three have $T = (Si + B)_6$ apfu; 14 have $T = (Si + Al)_6$ apfu; 18 have $T = (Si + B + Al)_6$ apfu; and seven have too high a content of paramagnetic species (and hence a degraded spectrum) to reliably detect minor Al and/or B (Table 3).

There is no clear-cut correspondence between the species

of tourmaline and whether either $^{[4]}$B or $^{[4]}$Al is present in the structure. Of course, we lack sufficient samples for some compositions (e.g., magnesiofoitite; Hawthorne et al. 1999) to state definitively that no pattern exists. Only in species in which the *Y* site is dominated by Mg (i.e., dravite, uvite, and magnesiofoitite) is $^{[4]}$Al consistently present and $^{[4]}$B consistently absent (and this is only for three of our samples). Within the elbaite-liddicoatite series, there seems to be no method of predicting the type of *T*-site occupancy, which is quite variable: $T = (Si, B)_6$, or $T = (Si, Al, B)_6$, but not $T = (Si, Al)_6$ apfu.

Although MAS NMR has proven a successful method of identifying the presence of tetrahedrally coordinated constituents in tourmaline with low contents of paramagnetic species, deriving quantitative results, particularly concerning Al site populations, is usually precluded by the fact that the spectral bands are subject to severe broadening by paramagnetic constituents.

Acknowledgments

This work was funded by an NSERC PGS-D to A.J.L. and V.K.M., by a Canada Research Chair in Crystallography and Mineralogy, and by Major Facilities Access grants to F.C.H., and by Research Tools and Equipment, and Discovery Grants to F.C.H. and S.K. from the Natural Sciences and Engineering Research Council of Canada, and by Canada Foundation for Innovation Grants to F.C.H. and S.K.

References cited

Aurisicchio, C., Ottolini, L., and Pezzotta, F. (1999) Electron- and ion-microprobe analyses, and genetic inferences of tourmalines of the foitite-schorl solid solution. European Journal of Mineralogy, 11, 217–225.

Bloodaxe, E.S., Hughes, J.M., Dyar, M.D., Grew, E.S., and Guidotti, C.V. (1999) Linking structure and chemistry in the Schorl-Dravite series. American Mineralogist, 84, 922–928.

Bray, P.J. (1999) NMR and NQR studies of boron in vitreous and crystalline borates. Inorganica Chimica Acta, 289, 158–173.

Bray, P.J., Edwards, J.O., O'Keefe, J.G., Ross, V.F., and Tatsuzaki, I. (1961) Nuclear magnetic resonance studies of ^{11}B in crystalline borates. Journal of Chemical Physics, 35, 435–442.

Burns, P.C., MacDonald, D.J., and Hawthorne, F.C. (1994) The crystal chemistry of manganese-bearing elbaite. Canadian Mineralogist, 32, 31–41.

Cempírek, J., Novàk, M., Ertl, A., Hughes, J.M., Rossman, G.R., and Dyar, M.D. (2006) Fe-bearing olenite with tetrahedrally coordinated Al from an abyssal pegmatite at Kutna Hora, Czech Republic: structure, crystal chemistry, optical and XANES spectra. Canadian Mineralogist, 44, 23–30.

Dyar, M.D., Taylor, M.E., Lutz, T.M., Francis, C.A., Robertson, J.D., Cross, L.M., Guidotti, C.V., and Wise, M. (1998) Inclusive chemical characterization of tourmaline: Mössbauer study of Fe valence and site occupancy. American Mineralogist, 83, 848–864.

Ertl, A. and Hughes, J.M. (2002) The crystal structure of aluminium-rich schorl overgrown by boron-rich olenite from Koralpe, Styria, Austria. Mineralogy and Petrology, 75, 69–78.

Ertl, A., Pertlik, F., and Berhardt, H.-J. (1997) Investigations on olenite with excess boron from the Koralpe, Styria, Austria. Anzeiger, 134, 3–10.

Ertl, A., Hughes, J.M., Brandstätter, F., Dyar, M.D., and Prasad, P.S.R. (2003) Disordered Mg-bearing olenite from a granitic pegmatite from Goslarn, Austria: A chemical, structural and infrared spectroscopic study. Canadian Mineralogist, 41, 1363–1370.

Ertl, A., Rossman, G.R., Hughes, J.M., Prowatke, S., and Ludwig, T. (2005) Mn-bearing "oxy-rossmanite" with tetrahedrally coordinated Al and B from Austria: Structure, chemistry, and infrared and optical spectroscopy study. American Mineralogist, 90, 481–487.

Ertl, A., Hughes, J.M., Prowatke, S., Ludwig, T., Prasad, P.S.R., Brandstatter, F., Korner, W., Schuster, R., Pertlik, F., and Marschall, H. (2006) Tetrahedrally coordinated boron in tourmalines from the liddicoatite-elbaite series from Madagascar: Structure, chemistry, and infrared spectroscopic studies. American Mineralogist, 91, 1847–1856.

Ertl, A., Hughes, J.M., Prowatke, S., Ludwig, T., Brandstatter, F., Korner, W., and Dyar, M.D. (2007) Tetrahedrally coordinated boron in Li-bearing olenite from "Mushroom" tourmaline from Momeik, Myanmar. Canadian Mineralogist, 45, 891–899.

Grice, J.D. and Ercit, T.S. (1993) Ordering of Fe and Mg in tourmaline: The correct formula. Neues Jahrbuch Mineralogie, Monatshefte, 165, 245–266.

Hawthorne, F.C. and Henry, D.J. (1999) Classification of the minerals of the tourmaline group. European Journal of Mineralogy, 11, 201–215.

Hawthorne, F.C., Selway, J.B., Kato, A., Matsubara, S., Shimizu, M., Grice, J.D., and Vajdak, J. (1999) Magnesiofoitite, □ (Mg_2Al) Al_6 (Si_6O_{18}) $(BO_3)_3$ $(OH)_4$, a new alkali-deficient tourmaline. Canadian Mineralogist, 37, 1439–1443.

Henry, D.J. and Dutrow, B.L. (1992) Tourmaline in low-grade clastic sedimentary rocks: An example of the petrogenetic potential of tourmaline. Contributions to Mineralogy and Petrology, 112, 203–218.

——— (1996) Metamorphic tourmaline and its petrologic application. In E.S. Grew and L.M. Anovitz, Eds., Boron: Mineralogy, Petrology, and Geochemistry, 33, p. 503–557. Reviews in Mineralogy and Geochemistry, Mineralogical Society of America, Chantilly, Virginia.

Henry, D.J. and Guidotti, C.V. (1985) Tourmaline as a petrogenetic indicator mineral: an example from the staurolite-grade metapelites of NW Maine. American Mineralogist, 70, 1–15.

Hughes, J.M., Ertl, A., Dyar, M.D., Grew, E., Shearer, C.K., Yates, M.G., and Guidotti, C. (2000) Tetrahedrally coordinated boron in tourmaline: boron-rich olenite from Stoffhutte, Koralpe, Austria. Canadian Mineralogist, 38, 861–868.

Hughes, K.-A., Hughes, J.M., and Dyar, M.D. (2001) Chemical and structural evidence for $^{[4]}$B ↔ $^{[4]}$Si substitution in natural tourmalines. European Journal of Mineralogy, 13, 743–747.

Hughes, J.M., Ertl, A., Dyar, M.D., Grew, E.S., Wieden-Beck, M., and Brandstatter, F. (2004) Structural and chemical response to varying $^{[4]}$B content in zoned Fe-bearing olenite from Koralpe, Austria. American Mineralogist, 89, 447–454.

Kalt, A., Schreyer, W., Ludwig, T., Prowatke, S., Berhardt, H.-J., and Ertl, A. (2001) Complete solid solution between magnesian schorl and lithian excess-boron olenite in a pegmatite from the Koralpe (eastern Alps, Austria). European Journal of Mineralogy, 13, 1191–1205.

Kirkpatrick, R.J. (1988) MAS NMR spectroscopy of minerals and glasses. In F.C. Hawthorne, Ed., Spectroscopic Methods in Mineralogy and Geology, 18, p. 341–403. Reviews in Mineralogy, Mineralogical Society of America, Chantilly, Virginia.

Kirkpatrick, R.J., Smith, K.A., Schramm, S., Turner, G., and Yang, W.-H. (1985) Solid-state nuclear magnetic resonance spectroscopy of minerals. Annual Reviews of Earth and Planetary Science, 13, 29–47.

Kirkpatrick, R.J., Oestrike, R., Weiss Jr., C.A., Smith, K.A., and Oldfield, E. (1986) High-resolution ^{27}Al and ^{29}Si NMR spectroscopy of glasses and crystals along the join $CaMgSi_2O_6$-$CaAl_2SiO_6$. American Mineralogist, 71, 705–711.

Klinowski, J., Carr, S.W., Tarling, S.E., and Barnes, P. (1987) Magic-angle-spinning NMR shows the aluminosilicate framework of ultramarine to be disordered. Nature, 330, 56–58.

Kroeker, S. and Stebbins, J.F. (2001) Three-coordinated boron-11 chemical shifts in borates. Inorganic Chemistry, 40, 6239–6246.

Kroeker, S., Neuhoff, P.S., and Stebbins, J.F. (2001) Enhanced resolution and quantitation from "ultrahigh" field NMR spectroscopy of glasses. Journal of Non-Crystalline Solids, 293–295, 440–445.

Lussier, A.J., Herwig, S., Abdu, Y., Hawthorne, F.C., Aguiar, P.M., Michaelis, V.K., and Kroeker, S. (2008a) Mushroom elbaite from the Kat Chay mine, Momeik, near Mogok, Myanmar: I. Crystal chemistry by SREF, EMPA, MAS NMR and Mössbauer spectroscopy. Mineralogical Magazine, 72, 747–761.

——— (2008b) Mushroom elbaite from the Kat Chay mine, Momeik, near Mogok, Myanmar: II. Zoning and crystal growth. Mineralogical Magazine, 72, 999–1010.

MacDonald, D.J. and Hawthorne, F.C. (1995) The crystal chemistry of Si-Al substitution in tourmaline. Canadian Mineralogist, 33, 849–858.

Marler, B. and Ertl, A. (2002) Nuclear magnetic resonance and infrared spectroscopic study of excess-boron olenite from Koralpe, Styria, Austria. American Mineralogist, 87, 364–367.

Marler, B., Borowski, M., Wodara, U., and Schreyer, W. (2002) Synthetic tourmaline (olenite) with excess boron replacing silicon in the tetrahedral site: II. Structure analysis. European Journal of Mineralogy, 14, 763–771.

Neiva, A.M.R., Manuela, M., Silva, V.G., and Gomes, M.E. (2007) Crystal chemistry of tourmaline from Variscan granites, associated tin-tungsten- and gold deposits, and associated metamorphic and metasomatic rocks from northern Portugal. Neues Jahrbuch Mineralogie Abhandlungen, 184, 45–76.

Novàk, M., Selway, J., Černý, P., Hawthorne, F.C., and Ottolini, L. (1999) Tourmaline of the elbaite-dravite series from an elbaite-subtype pegmatite at Blizna, southern Bohemia, Czech Republic. European Journal of Mineralogy, 11, 557–568.

Povondra, P. (1981) The crystal chemistry of tourmalines of the schorl-dravite series. Acta Universitatis Carolinae Geologica, 3, 223–264.

Povondra, P. and Novàk, M. (1986) Tourmalines in metamorphosed carbonate rocks from western Moravia, Czechoslovakia. Neues Jahrbuch Mineralogie, Monatshefte, 1986, 273–282.

Prowatke, S., Ertl, A., and Hughes, J.M. (2003) Tetrahedrally-coordinated Al in Mn-rich, Li- and Fe-bearing olenite from Eibenstein an der Thaya, Lower Austria: A chemical and structural investigation. Neues Jahrbuch für Mineralogie, Monatshefte, 2003, 385–395.

Schreyer, W., Wodara, U., Marler, B., van Aken, P.A., Seifert, F., and Robert, J.-L.

(2000) Synthetic tourmaline (olenite) with excess boron replacing silicon in the tetrahedral site: I. Synthesis conditions, chemical and spectroscopic evidence. European Journal of Mineralogy, 12, 529–541.

Schreyer, W., Hughes, J.M., Bernhardt, H.-J., Kalt, A., Prowatke, S. and Ertl, A. (2002) Reexamination of olenite from the type locality: detection of boron in tetrahedral coordination. European Journal of Mineralogy, 14, 935–942.

Selway, J., Černý, P., and Hawthorne, F.C. (1998) Feruvite from lepidolite pegmatites at Red Cross Lake, Manitoba. Canadian Mineralogist, 36, 433–439.

Selway, J.B., Novàk, M., Černý, P., and Hawthorne, F.C. (1999) Compositional evolution of tourmaline in lepidolite-subtype pegmatites. European Journal of Mineralogy, 11, 569–584.

——— (2000a) The Tanco pegmatite at Bernic Lake, Manitoba. XIII. Exocontact tourmaline. Canadian Mineralogist, 38, 869–976.

Selway, J.B., Černý, P., Hawthorne, F.C., and Novák, M. (2000b) The Tanco pegmatite at Bernic Lake, Manitoba. XIV. Internal tourmaline. Canadian Mineralogist, 38, 877–891.

Selway, J.B., Smeds, S.-A., Černý, P., and Hawthorne, F.C. (2002) Compositional evolution of tourmaline in the petalite-subtype Nyköpingsgruvan pegmatites, Utö, Stockholm Archipelago, Sweden. GFF, 124, 93–102.

Skibsted, J., Nielsen, N.C., Bildsøe, H., and Jakobsen, H.J. (1991) Satellite transitions in MAS NMR spectra of quadrupolar nuclei. Journal of Magnetic Resonance, 95, 88–117.

Tagg, S.L., Cho, H., Dyar, M.D., and Grew, E. (1999) Tetrahedral boron in naturally occurring tourmaline. American Mineralogist, 84, 1451–1455.

Taylor, M.C., Cooper, M.A., and Hawthorne, F.C. (1995) Local charge-compensation in hydroxyl-deficient uvite. Canadian Mineralogist, 33, 1215–1221.

Turner, G.L., Smith, K.A., Kirkpatrick, R.J., and Oldfield, E. (1986) Boron-11 nuclear magnetic resonance study of borate and borosilicate minerals and a borosilicate glass. Journal of Magnetic Resonance, 67, 544–550.

Manuscript received April 16, 2008
Manuscript accepted January 5, 2009
Manuscript handled by Bjorn Mysen